

Supporting Information
Resonance IR: A Coherent Multidimensional Analogue of
Resonance Raman

Erin S. Boyle, Nathan A. Neff-Mallon, Jonathan D. Handali, and John C. Wright

Department of Chemistry
University of Wisconsin-Madison
1101 University Avenue
Madison, WI 53706

Resonance Raman Spectrum in the Overtone Region:

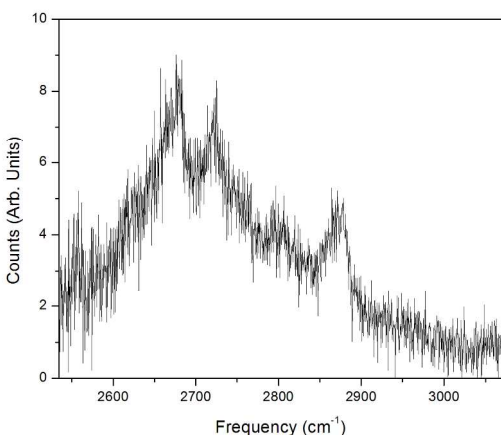


Figure S1. Resonance Raman of 1 mM $\text{Cu}(\text{tsPc})^{4-}$ in H_2O at 647 nm in the overtone region.

The overtone region displays peaks at 2676, 2723, and 2874 cm^{-1} , not corresponding with any of the transitions observed in the TRSF experiment. These may be overtones and combination bands of gerade or states, or unidentified fundamental modes. In either case it's clear the TRSF spectrum presents data not found in resonance Raman spectroscopy.

Infrared Absorption Spectrum:

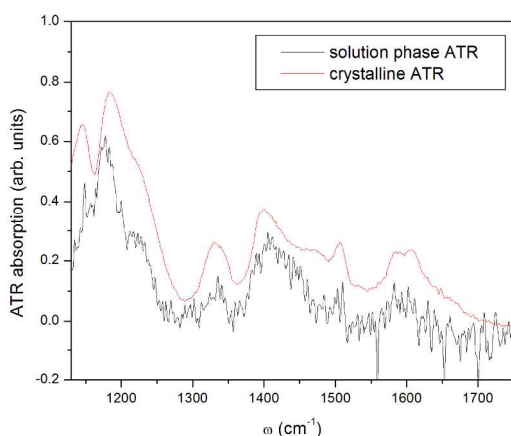


Figure S2. Attenuated total reflectance IR spectra of crystalline $\text{Na}_4\text{Cu}(\text{tsPc})$ and 26 mM $\text{Cu}(\text{tsPc})^{4-}$ in D_2O with solvent subtracted. Both have been rescaled arbitrarily for comparison.

To determine the transition strength of the infrared modes in $\text{Cu}(\text{tsPc})^{4-}$, the relative intensities of the D_2O 1212 cm^{-1} mode and the 1400 cm^{-1} $\text{Cu}(\text{tsPc})^{4-}$ mode were compared. The former was found to be 48.3x higher. Taking into account the relative molarities, 30 mM to 50.78 M, the molar absorptivity of the 1400 cm^{-1} mode is about 650 $\text{M}^{-1}\text{cm}^{-1}$. This was confirmed with a lower concentration in a transmission spectrum.

Time-dependent density functional theory (td-dft) results:

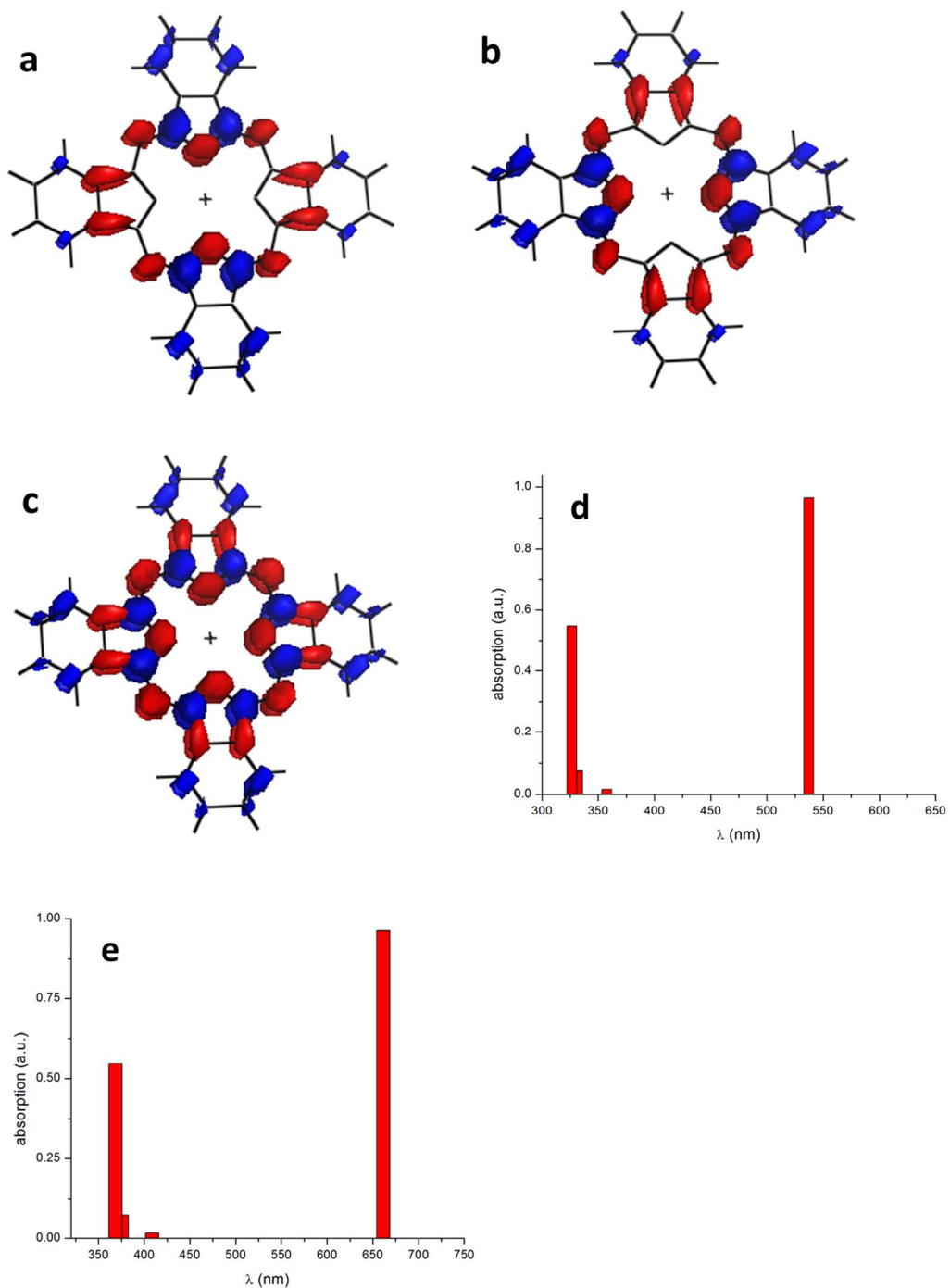


Figure S3. Electron density difference maps (EDDMs) plotted at an isosurface value of 0.001 au of (a) the first, and (b) the second of the degenerate CuPc Q-band transitions; (c) the overlay of both; (d) calculated absorption stick spectrum of CuPc; and (e) absorption stick spectrum of CuPc, downshifted by 3500 cm^{-1} .

Td-dft calculations performed on unsulfonated CuPc corroborate the spectroscopic result that vibrations located on the outer phenyl rings of CuPc are not significantly perturbed by the Q band electronic transition and therefore not well resonantly enhanced. Electron density difference maps of the two degenerate Q band transitions are shown in Fig. S3(a-c). While small electron density changes are observed on these outer rings, they are significantly smaller than those on the inner rings and contain only one phase, resulting in a smaller overall change in force on those nuclei. The td-dft results also indicate the Q band transition is essentially entirely ligand-based and therefore less susceptible to error. The absorption spectrum is fairly well reproduced by calculations (Fig. S3(d)). Because these calculations often result in linearly and positively shifted transition energies, the spectrum was downshifted by a typical value of 3500 cm^{-1} and replotted in wavelength space (Fig. S3(e)). The Q and Soret transitions then appear at 661 and 369 nm, as compared to their experimental values of 671 and 333 nm.

Overlay of TRSF and IR spectra and visible enhancement:

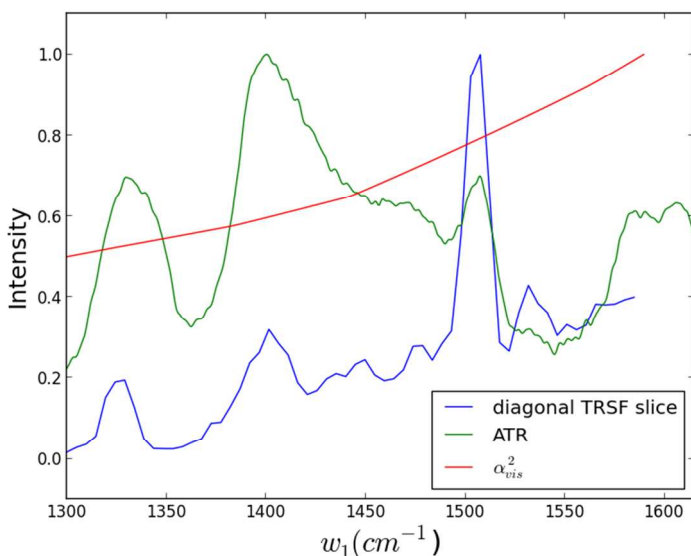


Figure S4. TRSF diagonal of Fig. 4, 5 mM $\text{Cu}(\text{tsPc})^{4-}$ in D_2O (blue); ATR spectrum of crystalline $\text{Na}_4\text{Cu}(\text{tsPc})$ (green); the square of the absorption cross-section of the Q band of $\text{Cu}(\text{tsPc})^{4-}$ at $2\omega_1+\omega_3$.

Fig. S4 overlays the diagonal trace of the $\text{Cu}(\text{tsPc})^{4-}$ TRSF spectrum, the ATR spectrum of solid $\text{Na}_4\text{Cu}(\text{tsPc})$, and the square of the absorption cross-section of the $\text{Cu}(\text{tsPc})^{4-}$ sample at the corresponding output frequency. The rise in background of the TRSF spectrum correlates well with the slope of the square of the absorption spectrum.

M-factors for TRSF:

Though output intensities in the TRSF experiments performed were high, small differences in the M-factor (Eq. 4) across the spectral range of our 2d data were observed. These differences have been modeled in order to compare to data absent of this experimental artifact. Though normal dispersion correctly assumes that the range of indices in the mid-IR will be lower than those in the visible, corrections to that trend must be made to account for perturbations to the index surrounding the vibrational resonances of the solvent and the electronic transition of the Cu(tsPc)⁴⁺. Absorption of the solvent in the mid-IR and the Cu(tsPc)⁴⁺ in the visible also play a role, but it is smaller.

Starting with an assumption of normal dispersion, phase-mismatch will be minimized in the most collinear geometry where the projections of \vec{k}_1 , \vec{k}_2 , and \vec{k}_3 are maximized, making their vector sum as large as possible and therefore closer in size to \vec{k}_4 . In our geometry, \vec{k}_3 enters normal to the sample with \vec{k}_1 and $\vec{k}_2 \pm \theta = 10^\circ$ to either side, resulting in a \vec{k}_4 output collinear with \vec{k}_3 . Indices of refraction in both the windows and the sample itself result in a change of input angle to θ_1 and θ_2 according to Snell's Law. Phase-mismatch then becomes:

$$\Delta k = 2\pi(n_1\omega_1 \cos(\theta_1) + n_2\omega_2 \cos(\theta_2) + n_3\omega_3 - n_4\omega_4). \quad (\text{S1})$$

This equation describes only vector mismatch in the direction of propagation, because mismatch in the x-plane (the sine projection) was found to be negligible. Indices of refraction of D₂O in the visible were taken from a Cauchy equation fit to experimental data by Odhner and Jacobs.¹ Indices of refraction of the solvent in the infrared were taken from Kramers-Kronig calculations done by John Bertie.² The latter indices had been given a constant offset based upon literature values at the time, but we altered that offset by -0.003 to match the Jacobs data. This has a minimal effect. The perturbation of the visible index due to Cu(tsPc)⁴⁺ was calculated following the equation

$$\Delta n(\omega) = \frac{\delta c \alpha}{2\omega \Gamma} \quad (\text{S2})$$

where $\delta = \omega - \omega_e$. In order to know δ , α , and Γ , the Cu(tsPc)⁴⁺ Q bands were fit to two Lorentzians (Fig. S5(a)), and the resulting parameters were used to find Δn (Fig. S5(b)). Final index values are shown in Fig S5(c). The resulting $\Delta k l / 2$ values are plotted in Fig S5(d). These values are under π , the location of the first node in $\text{sinc}^2(\frac{\Delta k l}{2})$ throughout the spectral range. The resulting M-factor is shown in Fig S5(e), and though it does impact signal at lower frequencies more significantly, it does not account for anywhere near the total trend in signal rise observed in Fig. 4, leading to the conclusion that electronic resonance is responsible for that trend.

Though Cu(tsPc)⁴⁺ Q bands contributed to phase-mismatch, their impact was relatively constant across the TRSF spectral range and therefore dampened the entire spectrum rather than

altering its relative intensities. Differences in relative intensities resulted from index perturbations in the IR due to the O-D bend, as well as slight absorption effects from the $\text{Cu}(\text{tsPc})^{4-}$ absorption.

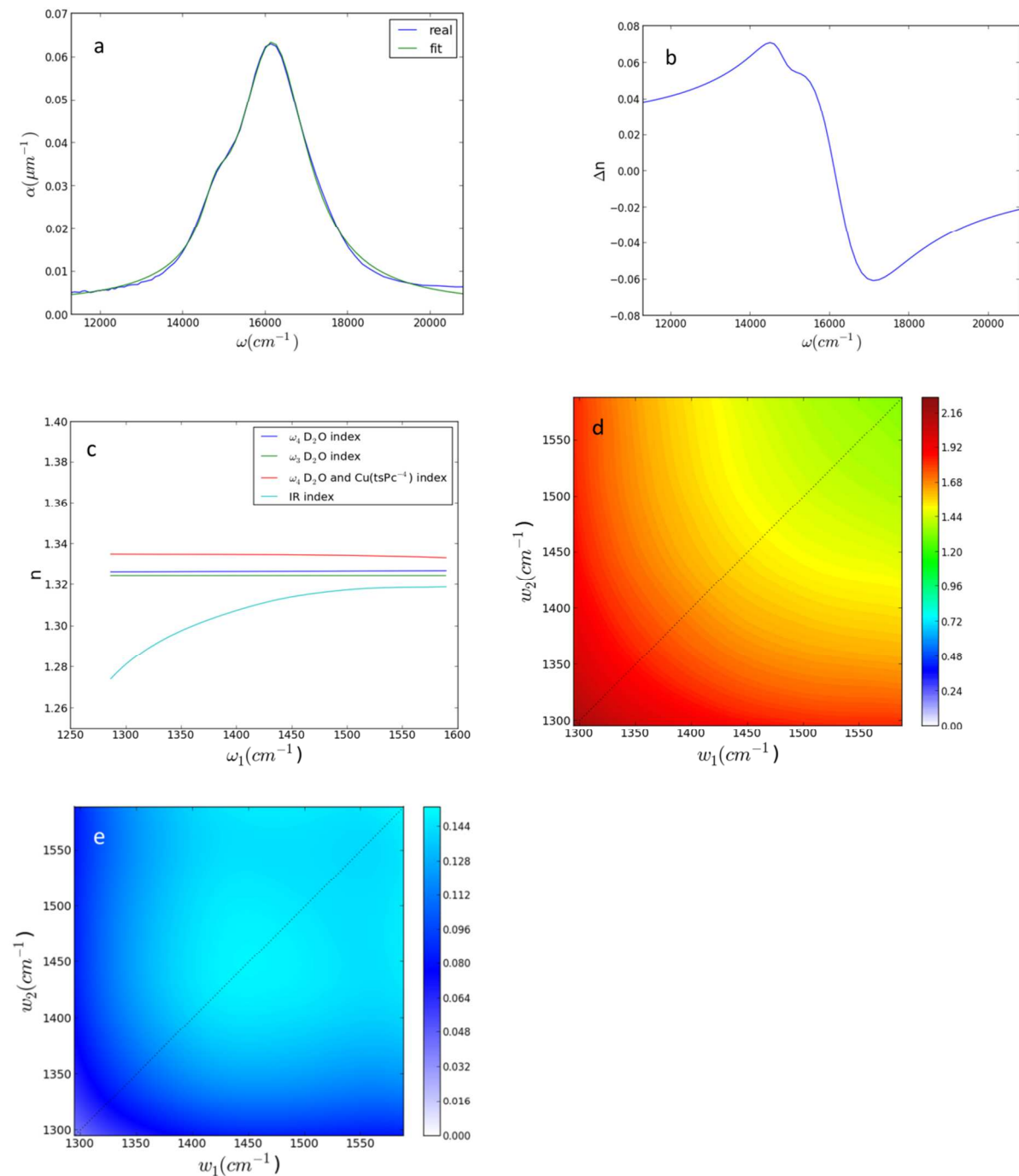


Figure S5. (a) Visible spectrum of $\text{Cu}(\text{tsPc})^{4-}$ Q bands and the two-Lorentzian fit; (b) index perturbation due to $\text{Cu}(\text{tsPc})^{4-}$ Q bands; (c) indices of ω_1 , ω_2 , ω_3 , and ω_4 across the TRSF range; (d) $\Delta kl/2$ at 25 μm pathlength; (e) M-factor for the TRSF experiment.

M-factors of fully vibrational four-wave mixing, for comparison:

Calculation of M-factors for fully infrared four-wave mixing in D₂O (phase matching $\vec{k}_1 - \vec{k}_2 + \vec{k}_3$ or $-\vec{k}_1 + \vec{k}_2 + \vec{k}_3$, nonrephasing or rephasing) were done in a completely analogous manner to the above. The calculations were performed both for the “pump-probe geometry” and the “boxcar geometry”. In the former, k_1 and k_2 are collinear, as are k_3 and k_4 . Because $\omega_1 = \omega_2$ and $\omega_3 = \omega_4$, this inherently removes phase-mismatch, leaving only absorption effects (Figs. S6(a,c)). In the boxcar geometry, k_1 and k_3 are at equal and opposite angles in the x-plane, while k_2 and k_4 are at equal and opposite angles in the y-plane (for the nonrephasing pathway). This results in imperfect cancellation since $\omega_1 \neq \omega_3$ and $\omega_2 \neq \omega_4$. Figs. S6(b,d) show the resulting M-factor at two path lengths. Fig. S6(e) shows the value of Δk , whose importance can be analyzed as growing as you approach the first node in $\text{sinc}^2(\Delta kl/2)$ when $\Delta kl/2 = \pi$.

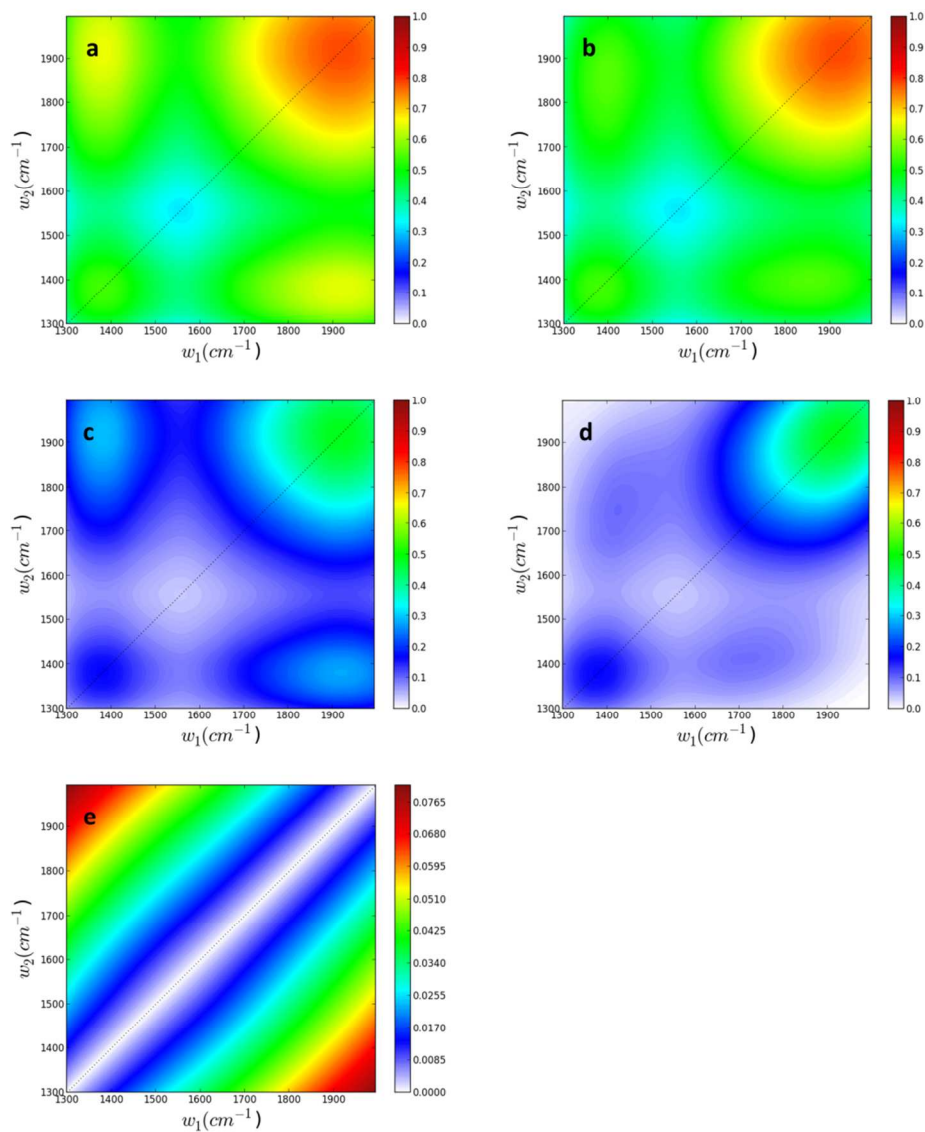


Figure S6. M-factors for a fully-vibrational four-wave mixing experiment in D₂O. (a) 25 μm, pump-probe geometry; (b) 25 μm, boxcar geometry at 5°; (c) 75 μm pump-probe geometry; (d) 75 μm boxcar geometry; (e) Δk , where $\Delta kl/2$ hits its first intensity node at π .

References:

1. Odhner, H.; Jacobs, D. T., Refractive Index of Liquid D₂O for Visible Wavelengths. *Journal of Chemical and Engineering Data* **2012**, *57* (1), 166-168.
2. Bertie, J. <http://www.ualberta.ca/~jbertye/JBDownload.HTM>.